RESEARCH ARTICLE

Vortex-induced vibration effect of extreme sea states over the structural dynamics of a scaled monopile offshore wind turbine

Juan Gabriel Rueda-Bayona[1] · Andrés Guzmán[2] · Juan José Cabello Eras[3]

Abstract

In order to demonstrate the relevance of considering Vortex-Induced Vibrations (VIV) in the structural design of marine structures, this study proposes an alternative experimental and analytical approach in wet conditions to measure the fluid–structure interaction in the near field and quantify the viscous damping with measured structural and 3D hydrodynamic accelerations. It was demonstrated that VIV caused and incremented 5.00% of the structural damping coefficient, and the extreme wind loading increased 74% of the offshore monopile's structural damping, demonstrating the relevance of the high non-linear hydrodynamics effects during selecting parameters into the structural design in offshore applications.

Keywords Vortex-induced vibrations · Fluid–structure interaction · Hydrodynamic field · Viscous damping · Offshore monopile

1 Introduction

The development of offshore engineering projects for non-conventional and marine energies shows worldwide growth, where offshore wind energy technology receives considerable financial resources for research and technological development (Rueda-Bayona et al. 2019). The offshore energy sector's opportunities bring challenges, such as the mitigation of environmental and economic impacts because of structural failures caused by extreme sea states (ESS) (Xie and Aly 2020). These hazards demand rigorous structural

design for developing effective damping systems and a better understanding of non-linear fluid–structure interactions. In this sense, the fluid–structure interaction of the hydrodynamic field of offshore monopile wind turbines has been studied, resulting in viscous damping that affects the structural dynamics, thus, in the structural design, vortex-induced vibrations (VIV) generated during extreme sea states are not commonly measured; its estimation for the structural design is relegated to hydrodynamic coefficients with a secondary contribution to the structural excitation frequencies. Also, offshore structural parameters have been identified in dry conditions through shakers and wind tunnels. The aforementioned common practice could be dangerous because structural amplifications may be ignored. After all, the VIV effects are not considered.

Several studies have analysed the effects of linear and nonlinear wind, waves, and currents loads over fixed structures, estimating the natural and damped period of the response (Aggarwal et al. 2017; Marino et al. 2017; Bajrić et al. 2018). Other studies highlighted that wind and wave loading mitigated vibrations of their offshore Monopile Wind Turbine (MWT) during earthquake excitations (Yang et al. 2020). As evidenced further, there is not a significant quantity of studies devoted to coupling physics considering loads acting simultaneously in the specialised literature. The environmental loads (wind, waves, and currents) have been one of the main

✉ Juan Gabriel Rueda-Bayona
  juan.gabriel.rueda@correounivalle.edu.co

  Andrés Guzmán
  faguzman@uninorte.edu.co

[1] Natural and Environmental Resources Engineering School (EIDENAR), Faculty of Engineering, Universidad del Valle, 25360 Cali, Colombia

[2] Research Group for Structures and Geotechnics (GIEG), Department of Civil and Environmental Engineering, Universidad del Norte, Km 5 Via Puerto Colombia, Bloque K, 8-33K, Barranquilla, Colombia

[3] Departamento de Ingeniería Mecánica, Facultad de Ingeniería, Universidad de Córdoba, Carrera 6 No. 77-305, Montería, Colombia

causes of accidents on-board and structural failures during the last decades provoking operational impairment of the offshore structures (Kandasamy et al. 2016). This explains why numerical and physical modelling to calculate the structural design parameters under complex non-linear environmental loading conditions have been widely studied in the design of the offshore structures (Jafarabad et al. 2014; Rueda-Bayona et al. 2018b).

Bachynski et al. (2019) assessed the structural response of a 5 MW offshore MWT under irregular wave loading. They evidenced that the numerical results overestimated the second-order wave excitation, miscalculated the third-order wave excitation, and incorrectly calculated the low structural damping. Other studies applied wave loads calculated from a synthetic-free surface generated by the JONSWAP spectra. These studies did not show details of the fluid–structure interaction because of the hydrodynamic vortex generated by the waves approaching the structure (Ou et al. 2007; Aggarwal et al. 2017; Zuo et al. 2017). Wei et al. (2017) estimated structural damping considering the effect of wave heights over structural deformations but omitted the effect of wave periods. Sun (2018) developed an analytical model of an MWT with a semi-active tuned mass damper for assessing the damping capacity during wind, waves, and earthquake excitations without a non-linear analysis among the structural responses and near-field excitations.

Arany et al. (2017) used a method for designing monopiles of an offshore wind turbine for defining types and sizes for financial viability, who pointed the application of linear wave theory for estimating mild and extreme wave loads. The method did not consider the critical structural responses caused by the fluid–structure non-linear interactions, because the calculation of hydrodynamic forces with the linear theory cannot determinate the complex structural responses which must be controlled with specialised viscous dampers. Suja-Thauvin et al. (et al. 2018) carried out numerical and physical modelling of a 4 MW wind turbine at model scale concluding that model assumptions and simplifications cause inaccuracies because of the overestimation of total structural responses, resulting in overinvestments in the offshore engineering project and cost overruns because of the increased repair and maintenance activities. These studies could be limited when simulating fluid–structure interactions, because CFD solvers might omit frequencies for exciting the first mode of structure oscillations (Paulsen et al. 2013). Although numerical modelling is fast and inexpensive for determining structural dynamic parameters in offshore structures, physical modelling with instrumented scaled models in tanks or wave channels (flumes) is strongly recommended.

Computational Fluid Dynamics (CFD) and numerical approaches are the most used methods to evaluate the non-linear responses of offshore structures because of wind, waves, and current loads (Lee and Mizutani 2009; Li et al.

2011; Rueda-Bayona et al. 2021). Colwell and Basu (Colwell and Basu 2009) applied the Kaimal and JONSWAP spectra to generate loads of wind and waves to assess the structural response of an offshore wind turbine. Wei et al. (2013) utilised the JONSWAP spectra to generate wave loads to develop a modal analysis of an offshore wind turbine considering the sea states in the Korean sea. Mockute et al. (2019) analysed numerically the exerted forces of combined and misaligned wind-wave loading over a MWT during rouge seas and reported that wave kinematics theoretical models did not capture properly the time evolution of loading force due to the local non-linear hydrodynamics. Although these approaches are relevant to consider non-linear responses, at that moment, these authors did not validate their models through experimental procedures.

Other studies have conducted physical modelling of offshore wind turbines in dry conditions using shakers or vibrating mechanisms in the absence of water (no wave flumes) (O'Kelly-Lynch et al. 2020). Ou et al. (2007) developed a damping isolation system to control vibrations of a jacket platform for determining structural parameters. Also, Mojtahedi et al. (2013) applied forced vibration tests with a shaker in dry conditions to analyse the structural health during several damage conditions. Hosseinlou and Mojtahedi (2016) assessed a physical scaled model of a jacket offshore structure through vibration tests in dry conditions to identify initial numerical parameters for structural health purposes. Jeong et al. (2020) developed a method in dry conditions for detecting structural damage near the bottom of a MWT; measured accelerations and angular velocity responses in order to identify critical natural frequencies of the structure because of wind and wave loading. Lin et al. (2020) analysed the structural dynamics of an offshore MWT scaled model in a wind tunnel and carried out dry tests omitting the hydrodynamic fluid–structure interactions.

Several studies built physical models of offshore structures and did not analyse the near hydrodynamic field of the structure during unperturbed and perturbed conditions (Mojtahedi et al. 2013; Jafarabad et al. 2014; Hosseinlou and Mojtahedi 2016). Suja-Thauvin et al. (2017) analysed experimental results of two offshore MWT scaled models (flexible and stiff), measuring the wave elevations and structural accelerations during several sea states generated by the JONSWAP spectra. Also, the free surface (wave loading) aside from the structure was measured and did not consider wind loading and not reported the damping ratios of the rigid monopile. Maes et al. (2018) analysed structural accelerations of a MWT under breaking wave loads. Wave elevations over the structure were measured and pointed out that they did not consider the hydrodynamic viscous effect because of the complexity of estimating the process. The loads were measured when the wave break over the structure, omitting the wave hydrodynamics (orbital velocities) and the

viscous effect of the nearby field. Shirzadeh et al. (2013) recommended an experimental study of the offshore structural behaviour under wind and waves loads and the contribution of wind damping. In addition, Esfeh and Kaynia (2020) recommended using realistic wind and wave experimental conditions for estimating structural dynamic parameters during the effect of liquefaction on the performance of monopile foundations.

Most research focussed on reducing vibrations because of fore-aft environmental loading (waves, wind earthquakes). Still, VIV may significantly affect the offshore wind turbine stability, which requires a comprehensive understanding of this turbulent loading (Jahangiri and Sun 2019). About the hydrodynamic viscous damping because of VIV, several studies have been applying numerical and physical modelling to analyse that fluid–structure interaction (Zdravkovich 1996; Liang et al. 2020). Zhao et al. (2017) performed 3D numerical modelling of VIV of a monopile structure under wave loading, evidencing that the vibration of the pile affects the near hydrodynamic field what could increase the number of generated vortices. Miles et al. (2017) analyse how a monopile foundation affected the measured hydrodynamic field by a 3D current profiler during wave and current loading. Roy et al. (2018) measured through a 3D current profiler the near-field hydrodynamics upstream of a monopile for understanding the turbulent flow structure in the wake region. Other studies analysed scour processes, because VIV around monopile foundations of offshore wind turbines (Nielsen et al. 2010; Guan et al. 2019).

Shirzadeh et al. (2013) analysed real-life measurements of environmental loading and structural responses of 3 MW offshore wind turbines, highlighting the relevance of the ambient vibration test for identifying structural dynamics parameters considering the hydrodynamic damping because of VIV. Also, Subbulakshmi et al. (2016) pointed out the relevance of hydrodynamic vortex over the structural damping. Their study pointed out that the soil effects reduce the structural natural frequency, but not considering the hydrodynamic viscous damping that could affect the structural dynamics. Other studies utilised the inertia coefficient (C_M) of the Morison equation and diffraction wave theory for considering the viscous damping effect of VIV during wave loading over monopile turbines (Brekke et al. 2005; Bisoi and Haldar 2014). Despite several methods for estimating the viscous terms generated by VIV, its calculation may be challenging. The coefficient selection from tables and curves may omit the inherent viscous effects that could provoke under-over estimations of the structural responses.

The literature review highlighted the improvement needed for understanding the effect of viscous damping over the structural dynamics of fixed offshore wind turbines. The applied numerical modelling does not properly consider the complex non-linear fluid–structure interactions, which generated over or underestimated structural dynamic parameters. The physical modelling use is widely reported in specialised literature using vibrating mechanisms in dry conditions (e.g., shakers, wind tunnels) for identifying structural dynamic parameters under the wind, waves, and earthquake loading. Although those experimental results showed success in their research objectives, dry mode without water may conceal critical structural frequencies. The experimental results retrieved from wave basins or flumes (wet conditions) used records of water elevation measured aside (wave loading), over the structure, or far from the near hydrodynamic field, which could omit the near-field viscous effect during the fluid–structure interaction.

To the best knowledge of the authors, there is no reported experimental research in wet conditions (wave flumes or basins) focused on the effect of extreme winds over structural dynamics during rough sea states. Despite of some researchers use physical modelling in dry conditions for assessing the extreme wind loads effects over offshore structures, that approach does not consider the real effect of viscous damping seen during experiments in wet conditions, hence, they did not compare the natural non-linear interactions between structural accelerations and near hydrodynamic field accelerations. The VIV studies showed numerical and experimental results of fluid–structure interactions, where CFD solvers with measured in situ velocities of waves and currents depicted the near hydrodynamic field. Most of these were applied for scouring and sediment transport around monopiles and analysed how structural vibrations perturbed the near hydrodynamic field. Then, it was not found studies focussed on the measured viscous effect of extreme wave and wind loading over the structural dynamics of an offshore MWT.

The present study proposes an alternative approach to determine the main structural dynamic parameters under extreme waves and wind loading in wet conditions. This study assessed the near hydrodynamic field upstream of the monopile and structural acceleration of the wind turbine for analysing the non-linear effect of wave-wind loads over the structure. In this sense, a Design of Experiment (DOE) and an Analysis of Variance (ANOVA) was performed to evaluate the response of structural damps and periods under the non-linear effects of VIV and extreme loading. This paper is organised starting with a description of the model set-up, continuing with the assessment of natural periods and damping coefficients for the modeled structure. In the next stage, the fluid–structure interaction is evaluated, and the near hydrodynamic field is analysed. In the end, we offered a discussion of the results and main conclusions related to non-linear interactions of the fluid–structure interactions seen in vortex-induced vibrations.

2 Methods

In order to identify natural and damped periods of the structure in dry and wet conditions, the research was developed following experimental and analytical phases: (1) Model set-up., (2) Design of Experiment (DOE), (3) Natural periods, (4) Damping coefficients, (5) Fluid–structure interaction, and (6) Near Hydrodynamic field analysis. The next sections will describe and depict the application of the proposed methodology.

2.1 Model set-up

The wave channel is 37.0 m long, 0.80 m wide, and 1.20 m deep and is at the Coastal and Ports Laboratory of the Universidad Nacional Autónoma de México. A dissipative beach with gravel rocks is at the end of the channel for reducing internal wave reflections (Fig. 1). The water level for the experiment was 0.20 m. Four water level sensors recording to 100 Hz were located every 1.76 m (characteristic wavelength) from the centroid of the wind turbine model. A 3D velocity profiler (Vectrino, www.nortekgroup.com) measured x, y and z wave orbital velocities with an 80 Hz measurement rate, and was set at 0.08 m upstream from the model with a vertical recording profile of 0.07 m from the bottom. The 2D Ultrasonic Velocity Profiler (UVP) measured x and z wave orbital velocities and was set 0.16 m upstream from the wind turbine. Finally, inside the model's hub was installed a triaxial accelerometer recording at 200 Hz (Fig. 2).

This study configured a pulling system (Chakrabarti 2005) integrated by a dynameter and a nylon cable to apply extreme wind loads to the structure. The traction loads were constant during the experiment (Condition 2), and the cables pulled back the wind blades simulating constant extreme winds (Fig. 2). Because of each run of the experiment lasted 30 s approximately, the pulley system is considered proper, because this elapsed time may be related to a wind gust. The implemented pulling system simulates the effect of extreme winds such as Hurricanes or wind-gusts over the blades. Because in the real wind turbine systems, the pitch control stops the blade rotation (feathered blades) during extreme winds, the implemented pulling mechanism allowed simulating these extreme weather conditions. The scale factor (variable) for the parameters depicted in the set-up (Fig. 2) followed Froude's law recommended for the physical modelling of offshore structures (Chakrabarti 2005). To complement the analysis of horseshoe vortex generation, the parameters D/λ was verified according to Hogben (Hogben 1978), and the Keulegan-Carpenter (KC) was calculated using the expression $KC = (H_s/D)\pi$ (Journée and Massie 2002). These non-dimensional parameters used the wave parameters (Hs, Tp, λ) generated by the paddle, hence drawbacks for obtaining proper parameters may occur when

Table 1 Set-up parameters of the experiment

	Scaling (S = 1:50)	Model	Prototype
Monopile diameter, D (m)	S	0.034	1.68
Water depth (m)	S	0.20	10.00
Rotor diameter (m)	S	0.33	16.50
Hub height (m)	S	0.83	41.50
Hs_1 (m)	S	0.08	4.00
Hs_2 (m)	S	0.05	2.50
Hs_3 (m)	S	0.01	0.50
Tp_1 (s)	$S^{0.5}$	1.10	7.77
Tp_2 (s)	$S^{0.5}$	0.80	5.65
Tp_3 (s)	$S^{0.5}$	0.70	4.94
KC_1	1:1	7.48	7.48
KC_2	1:1	4.67	4.67
KC_3	1:1	0.93	0.93
Characteristic wavelength, λ (m)	S	1.75	87.5
D/λ	1:1	0.019	0.019

The subscript denotes the three extreme sea states (i.e., $Hs_{1,2,3}$ and $Tp_{1,2,3}$)

residuals waves remain after experimental run; 15 min were considered between each run to prevent noise in the wave measurements. The geometry and kinematic features of the model and prototype model are listed in Table 1.

The results of KC and D/λ derived from the wave parameters (Table 1) suggest that the flow regime with Hs_1 will be in the inertia regime with no wave diffraction; then, the generation of horseshoe vortex nearby the MWT is highly probable.

The DOE has two experimental conditions, each one with 3 runs with two repetitions (9 runs in total), where Condition 1 gathers the parameters for irregular wave loading (JONSWAP spectra, gamma = 1) with no wind loading, and Condition 2 considers combined irregular waves + wind loading (Table 2).

The pulley system was disconnected during the runs of Condition 1 to avoid artificial damping

The wave parameters such as significant wave height (Hs) and peak period (Tp) are related to extreme wave events. They are numerically scaled considering the linear wave theory and wave channel restrictions. Hs and Tp are associated with sea states reported in the literature (Rueda-Bayona et al. 2018a, 2020; Qiao et al. 2020). The wind loading for each run simulates extreme winds generated by hurricanes, where 50 g = 54.85 m/s (197.45 km/h) represent a hurricane category 3,
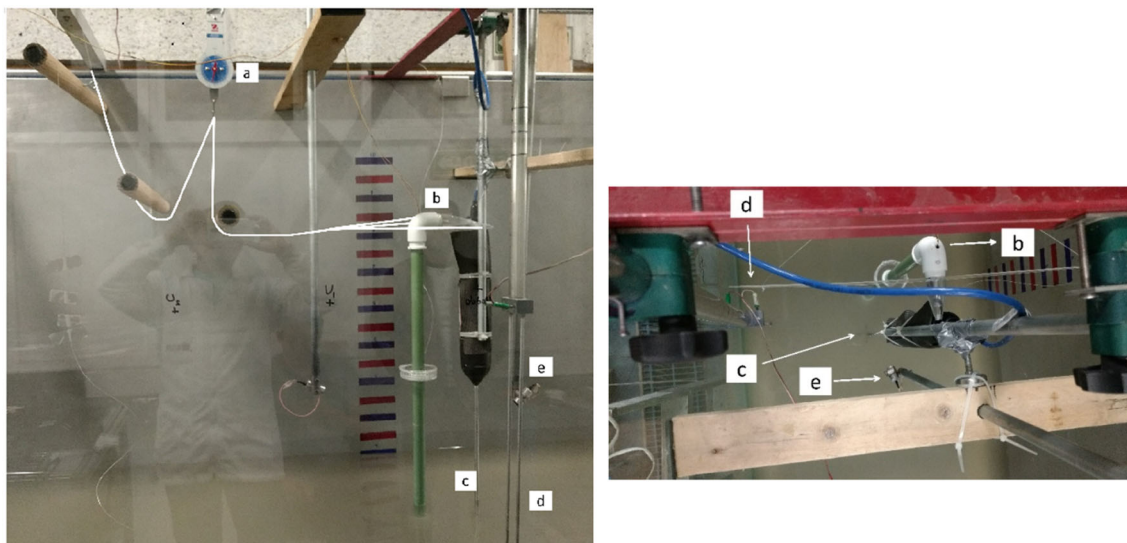
Lateral view:
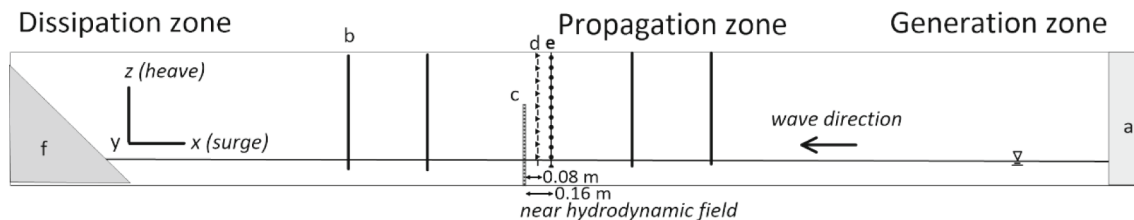
Cross-sectional view:
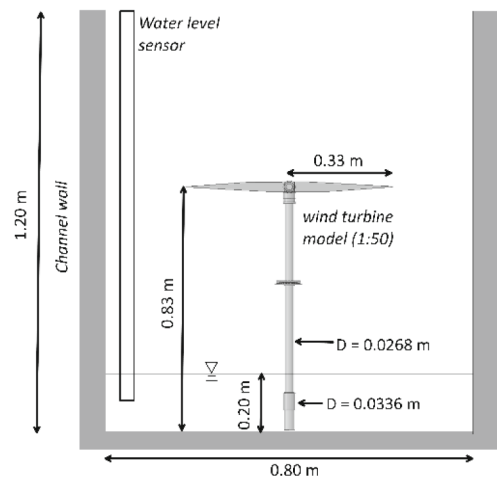
Fig. 1 Wave channel arrangement (lateral view) and wind turbine model (Cross-sectional view): **a** Wave paddle, **b** Water level sensor, c. wind turbine model, **d** 3D velocity sensor and water level sensor (aside), **e** Ultrasonic velocity profiler (UVP), **f** beach with gravel material

Fig. 2 Experiment set-up (lateral and top view): **a** dynameter, **b** accelerometer, **c** 3D velocity sensor, **d** water level sensor (SN), **e** 2D Ultrasonic velocity profiler (UVP). Drawn white lines represent the wind load mechanism

Table 2 Design of experiment (DOE)

Run	Condition 1 (no wind loading)			Condition 2			
	Extreme sea state	Hs (m)	Tp (s)	Run	Hs (m)	Tp (s)	Wind load (g)
1–3	1	0.08	1.1	10–12	0.08	1.1	50
4–6	2	0.05	0.8	13–15	0.05	0.8	150
7–9	3	0.01	0.7	16–18	0.01	0.7	250

150 g = 95 m/s (342 km/h) correspond to a hurricane category 5, and a wind load of 250 g = 122.65 m/s (441.54 km/h) simulates a strong hurricane category 5 (NWS-NOAA 2020).

The DOE-ANOVA method (DOE-ANOVA stands for Design of Experiments and the Statistical Analysis of Variance, based on significance tests of variables) and is applied frequently in coastal and offshore engineering in the analysis as run-up levels (Power et al. 2018), coastal protection (Hanley et al. 2014; Derschum et al. 2018), wave modelling (Rueda-Bayona et al. 2020) and structural dynamics of offshore structures (Rueda-Bayona et al. 2022).

This study identified the natural periods and damping coefficients through the logarithmic decrement and the half bandwidth methods (Chopra 2000; Cruciat and Ghindea 2012; Paz and Kim 2019). The logarithmic decrement has been applied to determine the critical damping of an offshore wind turbine foundation (Carswell et al. 2015) and oscillation modes (Koukoura et al. 2015). Van Der Tempel (2006) recommended the half bandwidth method for calculating the structural parameters in the design of support structures for offshore wind turbines.

3 Results and discussion

The structural response of a dynamic system is expressed in terms of its natural periods, damping coefficients and loads (fluid–structure interaction). This section discusses the findings related to this characterisation.

3.1 Natural periods

This study applied vibration tests in dry and wet conditions to identify the effect of hydrodynamic viscous damping. Five free vibration tests in dry conditions were run considering the x-dir degree of freedom (bending of the monopile in the x-direction), which is the main structural response because of the foundation restrictions and loading direction. The test comprised a controlled pulling (using a dynamometer) of the wind turbine hub with a cable and releasing it, for measuring the structural accelerations (a) as seen in Fig. 3.

The measured accelerations were utilised for calculating the natural period (Tn) and damping coefficient using the logarithmic decrement method. We performed five free vibration tests in dry conditions concluding that the structure has a natural period of 0.178 s (f = 5.6 Hz), along a damping of 0.081%.

The forced vibration test in wet conditions of this study consisted in the analysis of structural parameters of the turbine during the wave loading generated by the paddle, and wind effect produced by the pulley system. The test required a Fourier analysis for identifying the significant (mean) accelerations of loads and response accelerations derived from the measured hydrodynamic parameters and structural accelerations (x-direction), respectively. The zero spectral moment of accelerations (significant acceleration) and the associated period were selected to calculate the transfer functions and apply the half bandwidth method. Accordingly, six transfer functions were plotted using the x-dir accelerations and hydrodynamic loading measured during all the 9 runs (Table 2) by the water level sensor (SN – water surface elevation), the 3D velocity sensor (3DVS), and the 2D Ultrasonic velocity profiler (UVP); the acceleration loads were calculated using the free surface displacements measured by the SN, and the velocity records of 3DVS and UVP. The generated transfer functions have in the x-axis the load excitation frequency and in the y-axis the normalised acceleration $\left(\frac{\text{structural acceleration}}{\text{load acceleration}_{\text{SN, Vectrino, UVP}}}\right)$: the load excitation frequencies were calculated using the Fast Fourier Transform in the acceleration and period data.

The transfer function calculated through the SN records of the Condition 1 (Fig. 4) showed that wave load was between 0.9 Hz and 1.4 Hz, the hydrodynamic load measured by the 3DVS were 0.41 Hz and 1.6 Hz, and the load excitation frequency derived from UVP records where 0.27 Hz to 0.41 Hz. Then, the frequency of excitations in the near hydrodynamic field captured by the SN and the 3DVS were similar and doubled the frequencies captured by the UVP in the farthest field. In addition, the highest acceleration amplification was observed in the 3DVS's transfer functions, approximately 10,000 times higher than the transfer functions of SN and UVP with a peak frequency of 1.55 Hz.

The results for Condition 2 (waves + wind loading) evidenced damped curves because of the lower amplification of the normalised accelerations in the transfer curves (Fig. 4d–f). The transfer function derived from the UVP
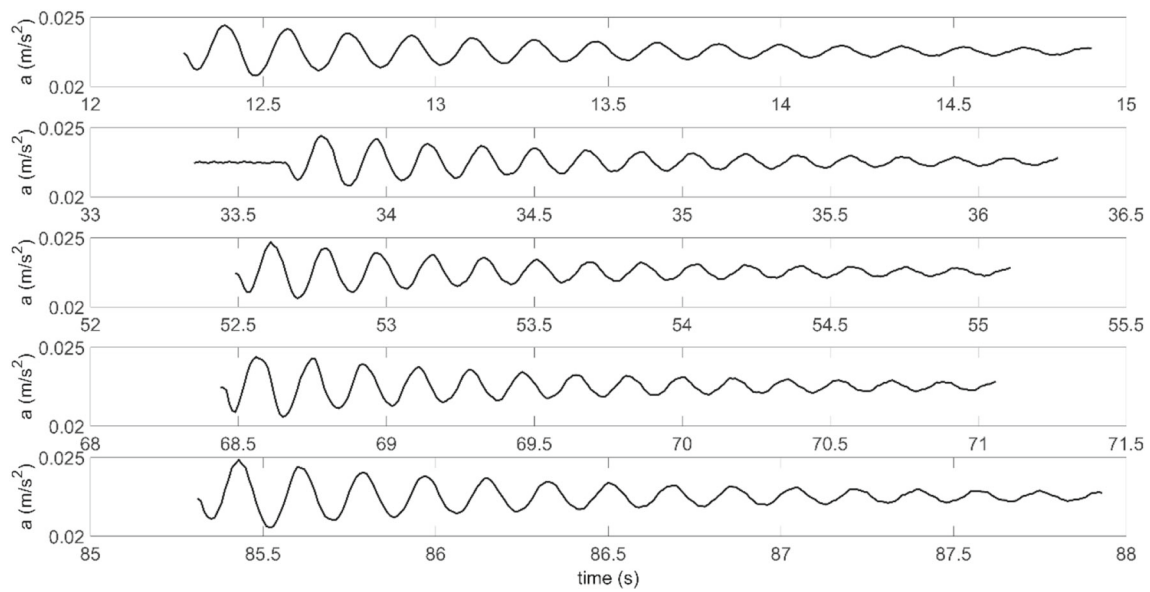
Fig. 3 Undisturbed free vibration test in dry conditions
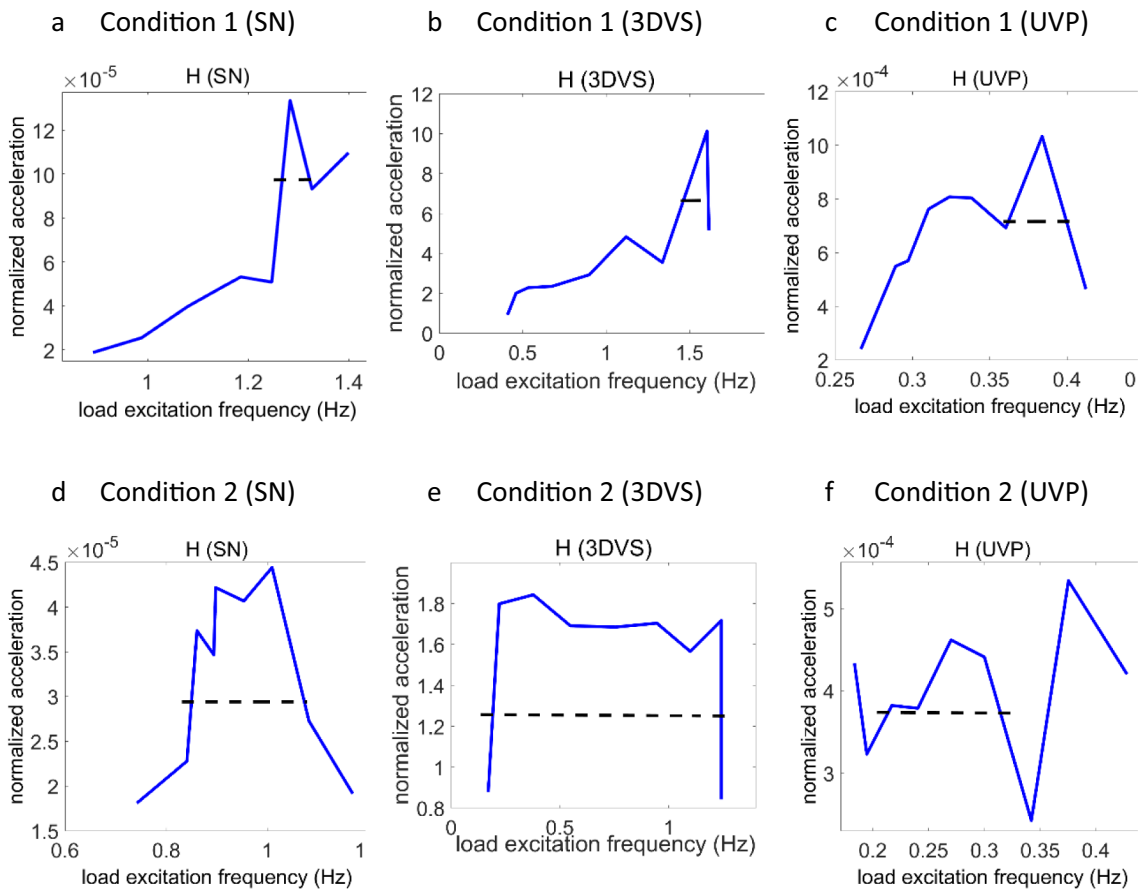
Fig. 4 Determination of damped natural periods through the half bandwidth method for Condition 1 (**a**, **b**, **c**) and Condition 2 (**d**, **e**, **f**)

records of Condition 2 (Fig. 4f) showed a normalised acceleration of 0.00025 with an irregular shape compared to the other transfer curves. However, because there were no reported anomalies in the UVP nor human errors, and the frequency range of the run was similar to the transfer function of Condition 1, this study considers that the high non-linear hydrodynamics generated the two amplification peaks of this transfer function (Fig. 4f).

The application of the half bandwidth method through the transfer function plots (Fig. 4) revealed the damped natural periods were associated with the forced vibration test. The dynamic parameters were then calculated using the hydrodynamic loads (HS, 3DVS, UVP), as shown in Table 3.

The damped natural periods (T_D) evidenced that UVP records reported the highest values from 2.61 s for Condition 1 and 3.70 s for Condition 2. The lowest damped period was identified using the 3DVS records during the Condition 1 period (T_D), which increased four times when the wind load was applied (Condition 2). The damped periods from SN were similar to 3DVS's in Condition 1, and it was observed no significant changes in T_D (0.99 s) when the wind load was applied. According to the previous results, this study considers that SN and UVP acceleration records are not affected by the near hydrodynamic field because of their higher periods and locations compared to the 3DVS (Fig. 2). It was also observed that the 3DVS's results evidenced the increment of 4-times in the damped period in Condition 2. Then, the applied wind load attenuated the structural vibrations and incremented T_D to 2.70 s.

3.2 Damping coefficients

The pseudo-acceleration response spectrum calculated with the free surface and flow accelerations (Fig. 5) pointed that acceleration peaks of 3DVS (Fig. 5a–c) were narrower than SN and UVP peaks (Fig. 5d–i). The 3DVS's results evidenced two spectra peaks at 0.05 s and 0.91 s; the UVP's results also showed two peaks with a higher magnitude but less differentiated between them compared to the 3DVS's results.

About the SN's results, they showed a single peak spectra similar to a bell curve. The SN's results did not capture two spectra peaks because its location compared to the other sensors (3DVS, UVP) was not in-line with the wave direction; thus, the accelerations were not affected by wave reflection during the fluid–structure interaction (wave loading).

The spectra curves of 3DVS and UVP evidence two spectra peaks generated by the non-linear interaction of the nearby hydrodynamic field. The 3DVS's results showed lower accelerations peaks because of its closer position to the structure compared to the UVP. The proximity of the 3DVS captured the highest viscous damping, mainly because of the hydrodynamic vortex generated in the near field. Then, the farthest

the hydrodynamics is measured at the foundation, the lower the hydrodynamic viscous damping is generated.

3.3 Fluid–structure interaction

Physical and hydrodynamic interactions, such as wave reflection-diffraction or changes in the near hydrodynamic field because of the generated vortex, may generate the non-linearities during the fluid–structure interaction. In this sense, to identify if the acceleration records of SN, 3DVS, and UVP captured the non-linearities mentioned above in the wave orbital velocities, a DOE-ANOVA analysis was performed.

The results of DOE-ANOVA were plotted in standardised effects bars and Pareto charts (Figs. 6 and 7), where each sensor was labelled as follows: A (3DVS), B (SN), C (UVP). A previous inspection of normalising or standardising the input data for modifying the x-axes of Pareto charts revealed that curve shapes did not change significantly; then, this study utilised variable x-axes derived from normalising with the highest record of each dataset (Figs. 6 and 7).

The DOE-ANOVA analysis derived from runs of Condition 1 evidenced the high nonlinearity in the acceleration results. Analysing the standardised effects graphs, only one second-order standardised effect seen in run 8 (Fig. 6o) proved that the factor AA (3DVS) influenced the structural acceleration (response). In this sense, the statistical relation (cause–effect) of fluid accelerations measured by the 3DVS with the structural acceleration was evidenced.

The ANOVA second-order effect of 3DVS's accelerations (AA) pointed out that when fluid accelerated and decelerated induced to the structure vibrating in the same load direction (x-dir). Then, the Pareto chart, in most of the runs (Fig. 6), evidenced the forward-backwards bending movements because of wave orbital velocities. The Pareto chart of run 8 (Fig. 6o) mentioned above supported the standardised effect of run 8, because the three convex curves were drawn. Despite run 7 and 9 are repetitions with the same experimental Conditions of run 8, the high nonlinearity involved allowed capturing the factor effect in one of the three same runs. In addition, the results of Fig. 6 evidenced that increasing the wave energy reduced the capability of DOE-ANOVA in identifying statistical evidence of the effect of factor (loading) over the response (structural accelerations).

The DOE-ANOVA analysis for Condition 2 (Fig. 7) with combined wind and wave loading showed more statistical significance compared to the DOE-ANOVA results of Condition 1 (Fig. 7).

The 3DVS's results revealed statistical significance in 4 of the 9 runs according to the standardised effects. The ANOVA second-order effects of the 3DVS (+ AA and − AA) were identified, which support the performed statistical analysis of Condition 1 (Fig. 6) and confirm that the calculated 3DVS's

Table 3 Damped natural periods (T_D), damping coefficients natural ($\omega_{1,2}$), and peak (ω_p) frequency derived from the application of the half bandwidth method

X-Direction	Ω_1 (HZ)	Ω_2 (HZ)	Ω_P, model (Hz)	Ω_P, prototype (Hz)	ζ	T_D (S)
Condition 1 (SN)	1.27	1.33	1.283	0.181	0.02	0.78
Condition 2 (SN)	0.69	1.075	1.009	0.143	0.21	0.99
Condition 1 (UVP)	0.364	0.397	0.383	0.054	0.04	2.61
Condition 2 (UVP)	0.24	0.32	0.270	0.038	0.14	3.70
Condition 1 (3DVS)	1.45	1.61	1.605	0.228	0.05	0.62
Condition 2 (3DVS)	0.19	1.25	0.370	0.052	0.74	2.70

accelerations influenced the structural dynamics of the structure. The + AA and −AA effects of runs 1, 2, 7, and 8 (Fig. 7a, c, m, o) showed the effect of acceleration and deceleration of wave orbital velocities over x-dir displacements of the structure. The Pareto chart's concave and convex curves reinforced the statement that wave orbital velocities in the near hydrodynamic field cause a high non-linear fluid–structure interaction.

Comparing the DOE-ANOVA results of Condition 1 and Condition 2 revealed that wind loading damped the structural dynamics because of the constant loading in the x-direction. The tilt of the wind turbine because of the aerodynamic loading controlled the x-dir displacements what reduced the normalised accelerations of the transfer functions (Fig. 4). Then, extreme wind loading revealed additional structural dynamic parameters that must be identified for dampers designing.

3.4 Near hydrodynamic field analysis

To verify the warning of generation of horseshoe vortex nearby the MWT (Table 1) and to analyse the non-linear effect of wave loading over the structure, were inspected the velocity records of Run 1—Condition 1 (Table 2) measured by the 3DVS (Fig. 8).

The measured horizontal and vertical velocities by the 3DVS of each 1 cm layer of a 7 cm profile (Fig. 8) allowed analysing the near hydrodynamic field (Fig. 8). The hydrodynamic field's initial records were close to 0 m/s because the experiment started with still water. From the 1000 records (10 s), the hydrodynamic field is excited, and from 1500 records, the x velocities showed positive and negative values associated with the in-line wave orbital velocities. The velocities from record 1500 to 4500 (30 s of elapsed time) pointed velocities about 0.2 m/s (negative and positive), where the velocities depicted a vertical vortex because of the x and z velocities.

In order to identify the mentioned above vortex because of the fluid–structure interaction, which induces viscous damping to the structure, this study zoomed in to the velocity measurements (Fig. 8) and extracted 0.3 s (26 records) of the time series (Fig. 9). As a result, positive horizontal x-velocities were detected from 16.4 to 16.7 s and negative values from 16.7 to 17.0 s, and positive values of vertical z-velocities in all the elapsed time. Then, horizontal x and z vertical component velocities evidenced an elliptical vortex (horseshoe vortex) with rotation, as seen in Fig. 9, which was warned by the KC and D/λ results of Table 1.

The spectral analysis of the velocity components measured by the 3DVS sensor (Fig. 10) revealed that x and z velocities have the same natural period (0.95 s); the horizontal y velocity reported a period of 0.003 s. The Strouhal (St) number was calculated using the mean in-line orbital velocity (0.2 m/s) and the vortex natural period (0.95 s), resulting in an intermediate St value of 0.18. The Re number also was calculated with a kinematic viscosity of 1×10^{-6} m^2/s, the mean in-line orbital velocity (0.2 m/s) and the monopile diameter (0.034 m), resulting in a value of 6720 for the model and 91,204 for the prototype. The St and Re results agreed with the St distribution of 0.2 in the range of $5 \times 10^{-2} < \text{Re} < 1 \times 10^5$ reported in other studies (Katopodes 2019; Tödter et al. 2021), where horseshoe vortex might appear. According to the time series inspection of wave orbital velocities (Fig. 9), the spectral analysis (Fig. 10) and the calculated St, KC and D/λ, a horseshoe vortex was identified governing the near hydrodynamic field of the MWT in this study.

Comparing the damped natural periods of Condition 1 (3DVS) reported in Table 3 against the velocity profiles measured nearby to the structure (Figs. 8 and 9), the spectral curve of 3D velocities (Fig. 10) and the vortex's period mentioned above (Fig. 9), it is evidenced that wind load increased the
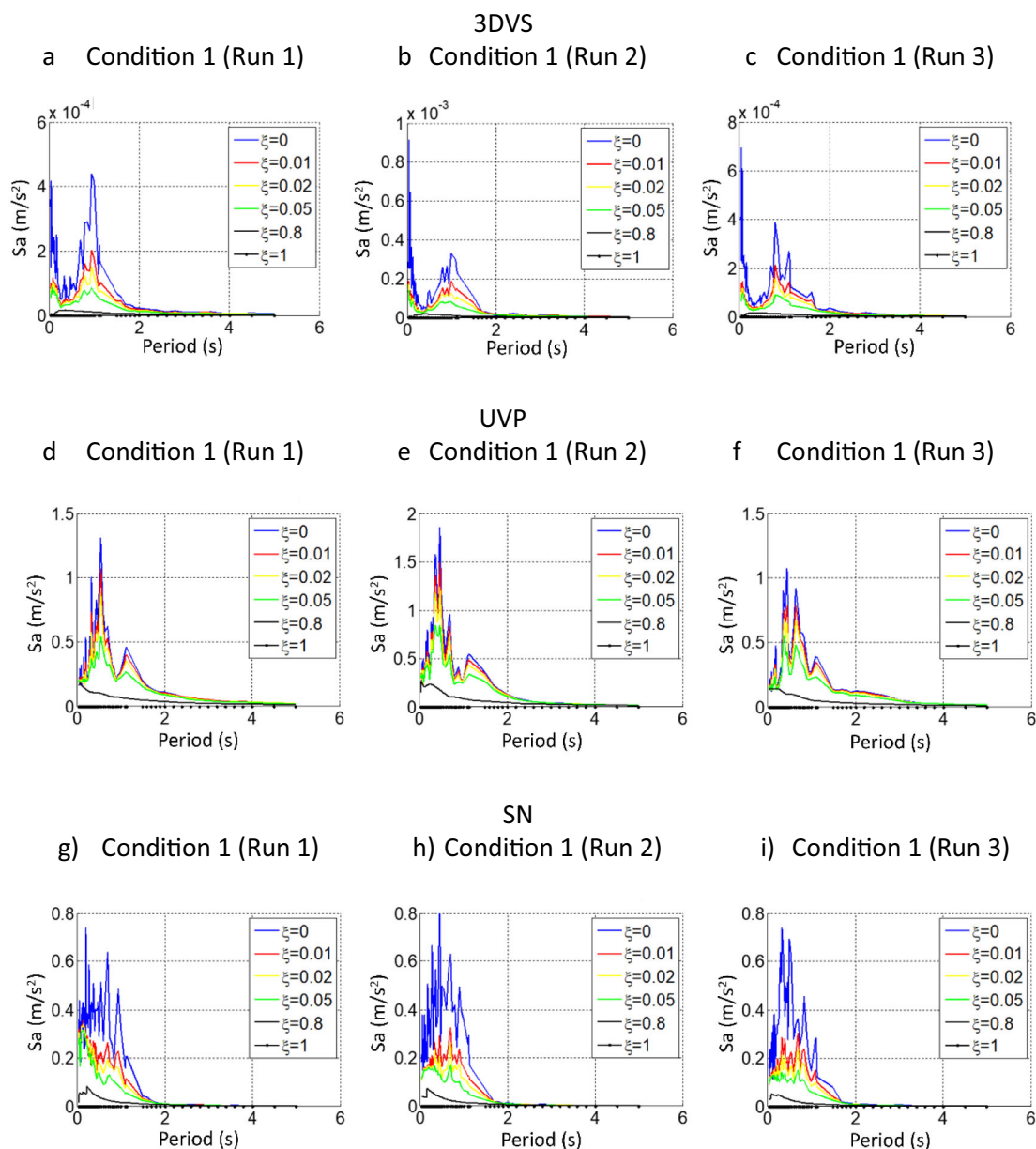
Fig. 5 Pseudo-acceleration response spectrum calculated by the Duhamel's integral derived from 3DVS (**a**, **b**, **c**), UVP (**d**, **e**, **f**) and SN (**g**, **h**, **i**) measurements. Free surface accelerations were calculated using the water level records (SN), and flow accelerations were calculated using the 3DVS and UVP records

structural damping and the vortex controlled the structural periods. As a result, the viscous damping generated at the near hydrodynamic field attenuated the hydrodynamic load over the structure. The natural periods of the structure in dry Conditions (Fig. 3) were 0.017 s and damped to 0.62 s (Condition 1–3DVS) during forced vibrations in wet Conditions (Table 3).

The increment of the natural period occurred by the wind load effect, and by the viscous effect of the nearby elliptical

vortex (Fig. 9) upstream of the structure, which controlled the structural vibration and damped the structure from 0.08% (dry conditions) to 5.00% (wet conditions) (Table 3). The increment of almost 5.00% of the damping coefficient of this study agrees with the relative differences between excitation frequencies and the natural frequency known as the over-5.00% criterion reported by the research of Ko Y.Y. (Ko 2020) and the guidelines of DNV-GL (DNV-GL 2016). The calculated 0.05% damping coefficient of Condition 1 (3DVS)

Fig. 6 Analysis of the fluid–structure interactions of all runs (**a-r**) of Condition 1 (irregular wave las loading) using the Pareto chart of standardised effects and main effects plots
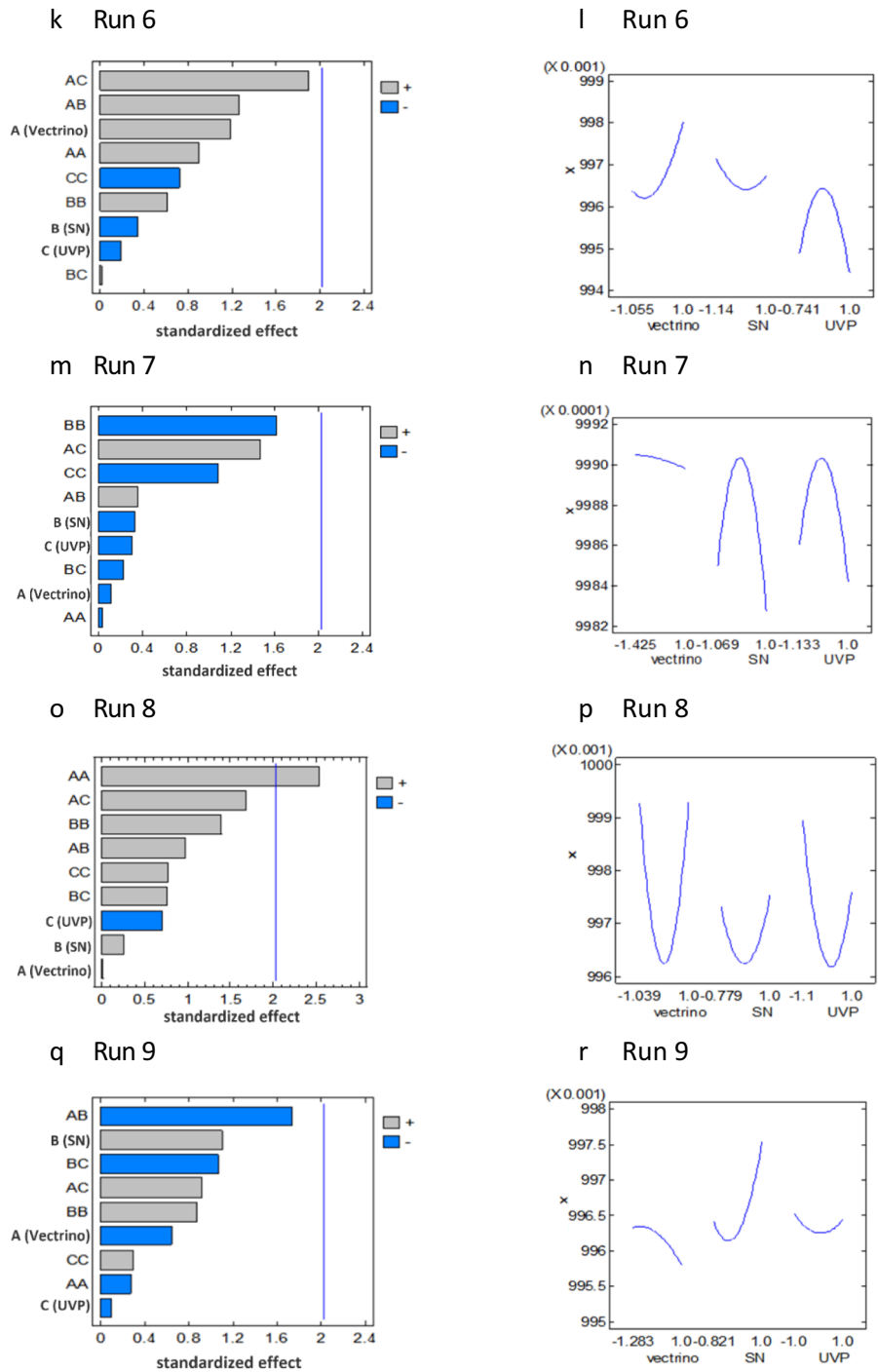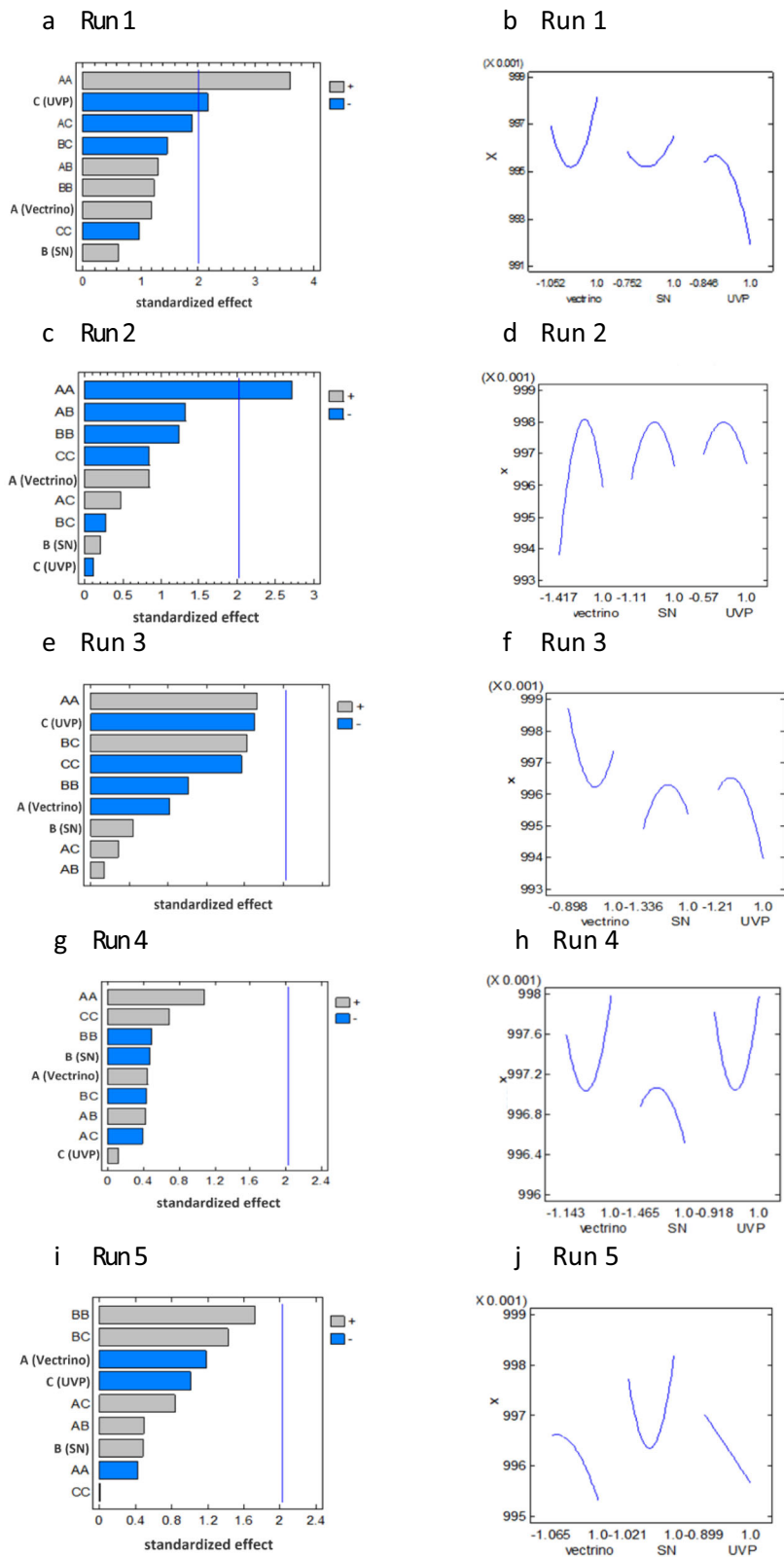
Fig. 6 continued

k Run 6

l Run 6

m Run 7

n Run 7

o Run 8

p Run 8

q Run 9

r Run 9
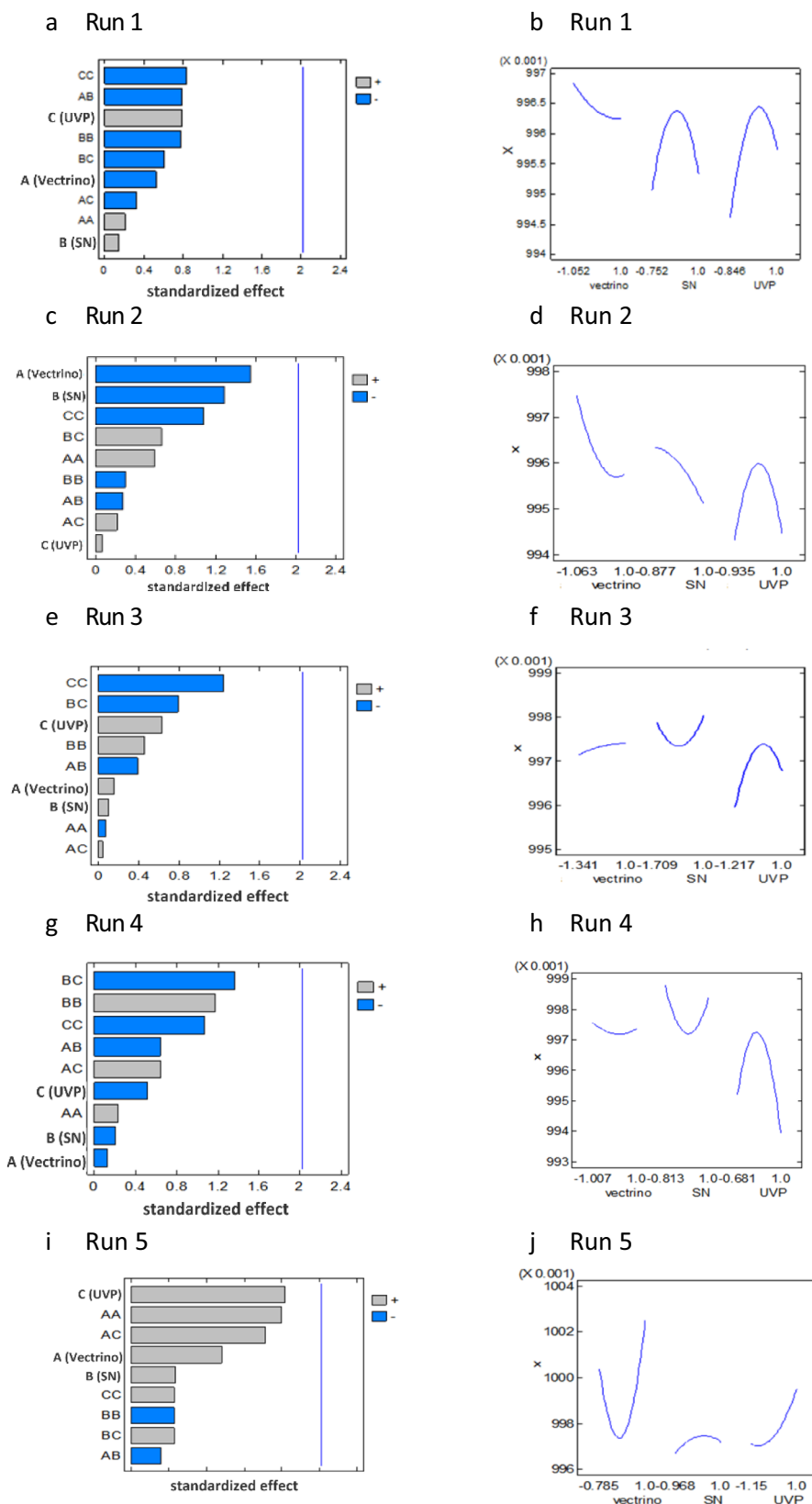
was similar to the hydrodynamic damping of 0.07% calculated by Shirzadeh et al. (Shirzadeh et al. 2013), who utilised in situ measurements of real ambient conditions of an operating MWT.

The normalised accelerations of the transfer functions (Fig. 4) evidenced that 3DVS's transfer curves reported the highest structural amplification, and the DOE-ANOVA analysis (Figs. 6 and 7) pointed out the statistical significance of the effect of 3DVS's accelerations over the structural accelerations (responses). As a result, it was proved the relevance of measuring at the near hydrodynamic field in front of the structure through the 3DVS. In this sense, the vortex generated by the fluid–structure interaction (Fig. 9) could not be captured by the water level sensor (SN), nor the 2D Ultrasonic velocity profiler (UVP) located farther from the structure (Fig. 2).

Fig. 7 Analysis of the fluid–structure interactions of all runs (**a-r**) of Condition 2 (irregular wave + wind loading) using the Pareto chart of standardised effects and main effects plots

Fig. 7 continued

k   Run 6

l   Run 6

m   Run 7

n   Run 7

o   Run 8

p   Run 8

q   Run 9

r   Run 9
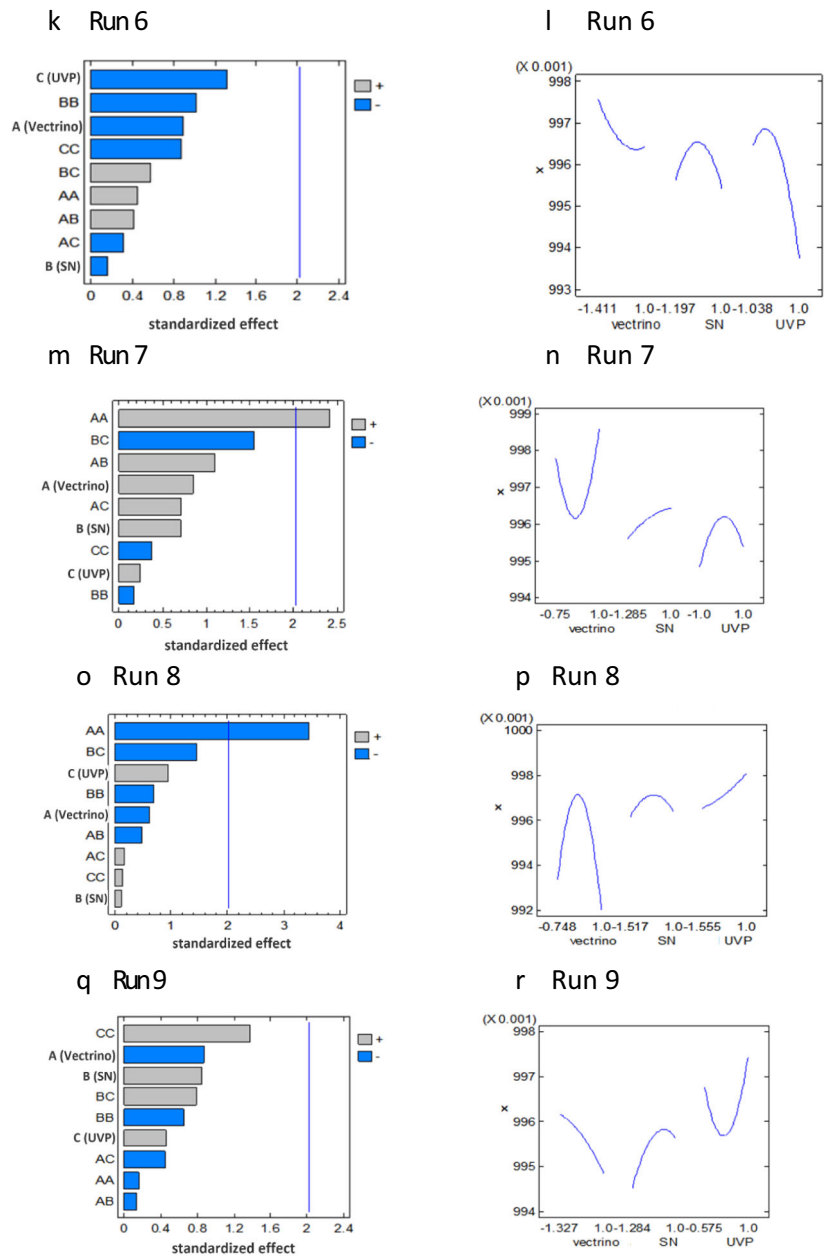
For preliminary stages of the structure, designing may use Pseudo-acceleration spectra curves (Fig. 5), where the fluid–structure interaction is not required for identifying damping coefficients. However, these spectra curves suggest a range of acceleration responses where the critical period (amplification-resonance) could be wrongly identified. However, these spectra curves may be considered for estimating the critical range of periods where the structure requires effective damping, which can be validated by the frequency ranges of the transfer curves and the calculated structural damped period through the application of the Half Bandwidth method in wet conditions.

Tödter et al. (2021) configured several physical experiments of a monopile under the effect of VIV, with the same geometry (diameter = 0.03 m) to this study, similar experimental conditions, and a different method known as 3D Digital Image Correlation (DIC). The authors reported a damping ratio of 0.0210 and a Strouhal number similar to the one found in this research (0.175). Miles et al. (2017) analysed the effect of VIV in MWT using a Vectrino Profiler Acoustic Doppler Velocimeter within a lab basin. The research used the Froude scaling for the experiments with similar wave parameters to the presented herein, with a different scale factor (1:25). These authors reported a similar
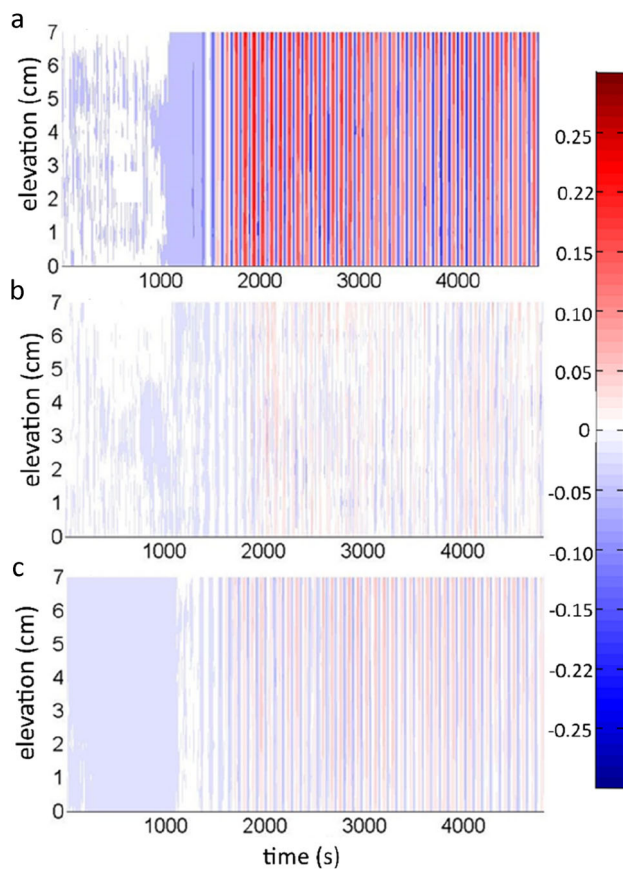
Fig. 8 3D velocity profiles measured by the 3DVS for the Run 1-Condition 1: **a** x-horizontal component **b** y- horizontal component **c** z-vertical component. The bottom level is pointed by the 0 cm of elevation (the lowest point of the profile), and the 7 cm level is the top of the profile.
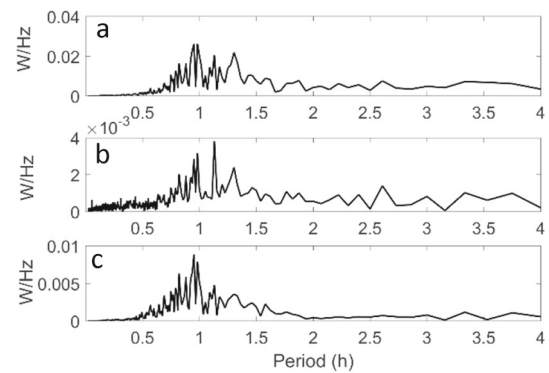

Fig. 10 Power spectral density curves calculated using 3DVS's records of **a** x-horizontal velocity, **b** y-horizontal velocity, **c** z-vertical velocity

KC (0.97) for the swell waves compared to the KC_3 from this study.

Previous research demonstrated the complexity of VIV (Tödter et al. 2021). Hence, the authors highlighted that research results strongly depend on structural parameters such as damping, geometry and structural parameters, which provoke different response amplitudes, frequencies and vortex patterns. In this sense, each OWT configuration will generate different structural parameters results. However, the damping ratio and Strouhal-KC numbers may be considered generalized parameters for structure design, no matter the ratio between models and prototypes. These parameters will keep the same, considering their non-dimensionality and defined limits. In this sense, the damping ratio calculated in this study applies to any scale between model and prototype.

In the common practice of offshore structure designing, it is assumed that structural damping may be determined in dry Conditions (e.g., shakers or vibrating tables) or through the mere utilisation of wave loads or measured velocity profiles
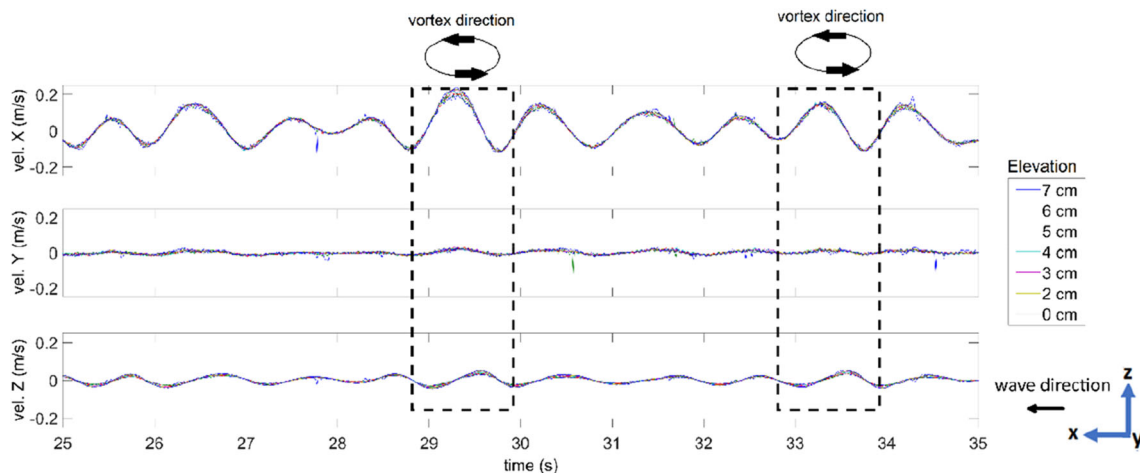
Fig. 9 Zoom in to the 3D velocity profiles measured by the 3DVS for the Run 1-Condition 1. The bottom level is pointed by the 0 cm of elevation (the lowest point of the profile), and the 7 cm level is the top of the profile

without the near fluid–structure interaction. It is then necessary for the offshore structure design to validate damped periods in wet Conditions and extreme excitations such as hurricane winds. The VIV and strong wind loading significantly modify the damped natural period.

4 Conclusions

The non-linear analysis of near-field fluid–structure interaction was performed after applying five steps or phases: (1) Model set-up, (2) Natural periods, (3) Damping coefficients, (4) Fluid–structure interaction, and (5) Near Hydrodynamic field analysis. As a result, each step revealed significant findings of the relevant effect of vortex-induced vibrations (VIV) over the structural dynamics of an offshore MWT.

The estimation of structural natural periods in dry conditions showed underestimations because of the calculated lower periods and damping coefficients compared to the dynamic parameters calculated in wet conditions.

The transfer function plots showed that normalised accelerations calculated using 3DVS's measurements were about 10,000 times higher compared to the transfer functions of SN and UVP. During irregular wave-wind loading, the transfer functions from 3DVS's records evidenced the increment of 4-times of the structural period compared to the transfer functions during solo irregular wave loading. It was evidenced that wind loading controlled the x-dir structural acceleration, damped the natural periods, and increased the damping coefficient.

The pseudo-acceleration response spectrums calculated through the water level sensor showed a single peak instead of two peaks. As a result, it was evidenced that utilising water level records measured aside from the structure will not capture the non-linearities of the near-field fluid–structure interactions, which will generate single-peaks spectra curves omitting different structural modes.

The DOE-ANOVA analysis confirms that the 3DVS's measurements captured VIV's non-linear effects over the structure, where a vertical vortex near the monopile foundation was detected. The identified vortex controlled the structural vibration during irregular wave loading and generated a damping coefficient of 0.05 according to the over-5.00% criterion, vortex which got intensified during the wind loading effect. The calculated damping ratios of this research and the identified effect of VIV over the structural dynamics, may be applicable to any scale between models and prototypes due to their non-dimensionality and defined limits.

The model scale used in this research may conceal excitation frequencies seen in real-life environments because of currents, then, the derived results of the study are limited to extreme sea states when the potential energy of waves heights predominates over the kinetic energy of ocean currents. For

future research, it is suggested to apply this methodology combining waves-wind-current loading in waves flumes to identify how currents affect the fluid–structure non-linear interactions.

Finally, this study recommends identifying dynamic parameters of offshore monopile foundations in wet conditions and measuring 3D velocities of the near hydrodynamic field to capture non-linear interactions of the fluid–structure interactions seen in vortex-induced vibrations.

References

1. Aggarwal N, Manikandan R, Saha N (2017) Nonlinear short term extreme response of spar type floating offshore wind turbines. Ocean Eng 130:199–209. https://doi.org/10.1016/j.oceaneng.2016.11.062

2. Arany L, Bhattacharya S, Macdonald J, Hogan SJ (2017) Design of monopiles for offshore wind turbines in 10 steps. Soil Dyn Earthq Eng 92:126–152. https://doi.org/10.1016/j.soildyn.2016.09.024

3. Bachynski E, Thys M, Delhaye V (2019) Dynamic response of a monopile wind turbine in waves: experimental uncertainty analysis for validation of numerical tools. Appl Ocean Res 89:96–114. https://doi.org/10.1016/j.apor.2019.05.002

4. Bajrić A, Høgsberg J, Rüdinger F (2018) Evaluation of damping estimates by automated operational modal analysis for offshore wind turbine tower vibrations. Renew Energy 116:153–163. https://doi.org/10.1016/j.renene.2017.03.043

5. Bisoi S, Haldar S (2014) Dynamic analysis of offshore wind turbine in clay considering soil-monopile-tower interaction. Soil Dyn Earthq Eng 63:19–35. https://doi.org/10.1016/j.soildyn.2014.03.006

6. Brekke J, Chakrabarti S, Halkyard J (2005) Drilling and production risers. Elsevier Ltd, Amsterdam

7. Carswell W, Johansson J, Løvholt F, Arwade SR, Madshus C, DeGroot DJ, Myers AT (2015) Foundation damping and the dynamics

of offshore wind turbine monopiles. Renew Energy 80:724–736. https://doi.org/10.1016/j.renene.2015.02.058

8. Chakrabarti SK (2005) Chapter 13 Physical Modelling of Offshore Structures. Elsevier, Amsterdam. https://doi.org/10.1016/B978-0-08-044381-2.50020-5

9. Chopra A (2000) Dynamics of structures: theory and applications to earthquake engineering, 2nd edn. Elsevier

10. Colwell S, Basu B (2009) Tuned liquid column dampers in offshore wind turbines for structural control. Eng Struct 31:358–368. https://doi.org/10.1016/j.engstruct.2008.09.001

11. Cruciat R, Ghindea C (2012) Experimental determination of dynamic characteristics of structures. Math Model Civil Eng 4:51–59

12. Derschum C, Nistor I, Stolle J, Goseberg N (2018) Debris impact under extreme hydrodynamic conditions part 1: Hydrodynamics and impact geometry. Coast Eng 141:24–35. https://doi.org/10.1016/j.coastaleng.2018.08.016

13. DNV-GL (2016) Support structures for wind turbines - DNVGL-ST-0126. https://www.dnv.com/energy/standardsguidelines/dnv-st-0126-support-structures-for-wind-turbines.html

14. Esfeh PK, Kaynia AM (2020) Earthquake response of monopiles and caissons for offshore wind turbines founded in liquefiable soil. Soil Dyn Earthq Eng 136:106213. https://doi.org/10.1016/j.soildyn.2020.106213

15. Guan D, Chiew YM, Melville BW, Zheng J (2019) Current-induced scour at monopile foundations subjected to lateral vibrations. Coast Eng 144:15–21. https://doi.org/10.1016/j.coastaleng.2018.10.011

16. Hanley ME, Hoggart SP, Simmonds DJ, Bichot A, Colangelo MA, Bozzeda F, Heurtefeux H, Ondiviela B, Ostrowski R, Recio M, Trude R (2014) Shifting sands? Coastal protection by sand banks, beaches and dunes. Coast Eng 87:136–146. https://doi.org/10.1016/j.coastaleng.2013.10.020

17. Hogben N (1978) Wave loads on structures. Mar Sci Commun 4:89–119. https://doi.org/10.1002/9781119241652.ch7

18. Hosseinlou F, Mojtahedi A (2016) Developing a robust simplified method for structural integrity monitoring of offshore jacket-type platform using recorded dynamic responses. Appl Ocean Res 56:107–118. https://doi.org/10.1016/j.apor.2016.01.010

19. Jafarabad A, Kashani M, Parvar MRA, Golafshani AA (2014) Hybrid damping systems in offshore jacket platforms with floatover deck. J Constr Steel Res 98:178–187. https://doi.org/10.1016/j.jcsr.2014.02.004

20. Jahangiri V, Sun C (2019) Integrated bi-directional vibration control and energy harvesting of monopile offshore wind turbines. Ocean Eng 178:260–269. https://doi.org/10.1016/j.oceaneng.2019.02.015

21. Jeong S, Kim EJ, Park JW, Shin DH (2020) Data fusion-based damage identification for a monopile offshore wind turbine structure using wireless smart sensors. Ocean Eng 195:106728. https://doi.org/10.1016/j.oceaneng.2019.106728

22. Journée JMJ, Massie WW (2002) Offshore hydromechanics. Delft University of Technology. First Edition. https://ocw.tudelft.nl/wp-content/uploads/Introduction_Offshore_Hydromechanics.pdf

23. Kandasamy R, Cui F, Townsend N, Foo CC, Guo J, Shenoi A, Xiong Y (2016) A review of vibration control methods for marine offshore structures. Ocean Eng 127:279–297. https://doi.org/10.1016/j.oceaneng.2016.10.001

24. Katopodes ND (2019) Viscous fluid flow. Free-Surface Flow. Butterworth-Heinemann, Oxford, pp 324–426

25. Ko Y-Y (2020) A simplified structural model for monopile-supported offshore wind turbines with tapered towers. Renew Energy 156:777–790. https://doi.org/10.1016/j.renene.2020.03.149

26. Koukoura C, Natarajan A, Vesth A (2015) Identification of support structure damping of a full scale offshore wind turbine in

27. Lee K-H, Mizutani N (2009) A numerical wave tank using direct-forcing immersed boundary method and its application to wave force on a horizontal cylinder. Coast Eng J 51:27–48. https://doi.org/10.1142/s0578563409001928

28. Li M, Zhang H, Guan H (2011) Study of offshore monopile behaviour due to ocean waves. Ocean Eng 38:1946–1956. https://doi.org/10.1016/j.oceaneng.2011.09.022

29. Liang B, Du S, Pan X, Zhang L (2020) Local scour for vertical piles in steady currents: review of mechanisms, influencing factors and empirical equations. J Mar Sci Eng 8:4. https://doi.org/10.3390/jmse8010004

30. Lin K, Xiao S, Zhou A, Liu H (2020) Experimental study on long-term performance of monopile-supported wind turbines (MWTs) in sand by using wind tunnel. Renew Energy 159:1199–1214. https://doi.org/10.1016/j.renene.2020.06.034

31. Maes K, Weijtjens W, de Ridder EJ, Lombaert G (2018) Inverse estimation of breaking wave loads on monopile wind turbines. Ocean Eng 163:544–554. https://doi.org/10.1016/j.oceaneng.2018.05.049

32. Marino E, Giusti A, Manuel L (2017) Offshore wind turbine fatigue loads: the influence of alternative wave modeling for different turbulent and mean winds. Renew Energy 102:157–169. https://doi.org/10.1016/j.renene.2016.10.023

33. Miles J, Martin T, Goddard L (2017) Current and wave effects around windfarm monopile foundations. Coast Eng 121:167–178. https://doi.org/10.1016/j.coastaleng.2017.01.003

34. Mockute A, Borri C, Marino E, Lugni C (2019) Wind-wave loading and response of OWT monopiles in rough seas. Lect Notes Civil Eng 27:507–518. https://doi.org/10.1007/978-3-030-12815-9_39/COVER

35. Mojtahedi A, Yaghin ML, Ettefagh MM, Hassanzadeh Y, Fujikubo M (2013) Detection of nonlinearity effects in structural integrity monitoring methods for offshore jacket-type structures based on principal component analysis. Mar Struct 33:100–119. https://doi.org/10.1016/j.marstruc.2013.04.007

36. Nielsen AW, Sumer BM, Fredsoe J, Christensen ED (2010) Scour protection around offshore wind turbines: Monopiles. In: Geotechnical Special Publication

37. NWS-NOAA (2020) Saffir-Simpson Hurricane Wind Scale. https://www.weather.gov/mfl/saffirsimpson. Accessed 3 Jun 2020

38. O'Kelly-Lynch P, Long C, McAuliffe FD et al (2020) Structural design implications of combining a point absorber with a wind turbine monopile for the east and west coast of Ireland. Renew Sustain Energy Rev 119:109583. https://doi.org/10.1016/j.rser.2019.109583

39. Ou J, Long X, Li QS, Xiao YQ (2007) Vibration control of steel jacket offshore platform structures with damping isolation systems. Eng Struct 29:1525–1538. https://doi.org/10.1016/j.engstruct.2006.08.026

40. Paulsen BT, Bredmose H, Bingham HB, Schløer S (2013) Steep wave loads from irregular waves on an offshore wind turbine foundation: computation and experiment. In: Conference proceedings international conference on offshore mechanics and arctic engineering. Honoring symposium on marine hydrodynamics. Am Soc Mech Eng Digital Collect, Nantes, France, p 10

41. Paz M, Kim YH (2019) Structural dynamics: theory and computation, 6th edn. Springer, Cham, Switzerland

42. Power HE, Gharabaghi B, Bonakdari H et al (2018) Prediction of wave runup on beaches using gene-expression programming and empirical relationships. Coast Eng 144:47–61. https://doi.org/10.1016/j.coastaleng.2018.10.006

43. Qiao C, Myers AT, Arwade SR (2020) Characteristics of hurricane-induced wind, wave, and storm surge maxima along the U.S.

Atl Coast Renew Energy 150:712–721. https://doi.org/10.1016/j.renene.2020.01.030

44. Roy S, Debnath K, Mazumder BS (2018) Distribution of turbulent eddies behind a monopile for vortex lock-on condition due to wave current combined flow. Coast Eng 131:70–87. https://doi.org/10.1016/j.coastaleng.2017.10.010

45. Rueda-Bayona JG, Eras JJC, Schneider I (2018a) Wind-Speed modelling using fourier analysis and nonlinear autoregressive neural network (NAR). In: Giannetti BF, Almeida CMVB, Agostinho F (eds) Advances in Cleaner production, proceedings of the 7th international workshop. Springer, Barranquilla, pp 1–198

46. Rueda-Bayona JG, Osorio-Arias A, Guzmán A, Rivillas-Ospina G (2018b) Alternative method to determine extreme hydrodynamic forces with data limitations for offshore engineering. J Waterw Port Coast Ocean Eng 145:16. https://doi.org/10.1061/(asce)ww.1943-5460.0000499

47. Rueda-Bayona JG, Guzmán A, Eras JJ, Silva-Casarín R, Bastidas-Arteaga E, Horrillo-Caraballo J (2019) Renewables energies in Colombia and the opportunity for the offshore wind technology. J Clean Prod 220:529–543. https://doi.org/10.1016/j.jclepro.2019.02.174

48. Rueda-Bayona JG, Guzmán A, Cabello Eras JJ (2020) Selection of JONSWAP spectra parameters during water-depth and sea-state transitions. J Waterw Port Coast Ocean Eng 146:04020038. https://doi.org/10.1061/(asce)ww.1943-5460.0000601

49. Rueda-Bayona JG, Gil L, Calderón JM (2021) CFD-FEM modeling of a floating foundation under extreme hydrodynamic forces generated by low sea states. Math Model Eng Probl 8:888–896. https://doi.org/10.18280/MMEP.080607

50. Rueda-Bayona JG, Guzmán A, Osorio AF (2022) DOE-ANOVA for identifying the effect of extreme sea-states over the structural dynamic parameters of a floating structure. Math Model Eng Probl 9:839–848. https://doi.org/10.18280/MMEP.090334

51. Shi W, Park H, Han J, Na S, Kim C (2013) A study on the effect of different modeling parameters on the dynamic response of a jacket-type offshore wind turbine in the Korean Southwest Sea. Renew Energy 58:50–59. https://doi.org/10.1016/j.renene.2013.03.010

52. Shirzadeh R, Devriendt C, Bidakhvidi MA, Guillaume P (2013) Experimental and computational damping estimation of an offshore wind turbine on a monopile foundation. J Wind Eng Ind Aerodyn 120:96–106. https://doi.org/10.1016/j.jweia.2013.07.004

53. Subbulakshmi A, Sundaravadivelu R (2016) Heave damping of spar platform for offshore wind turbine with heave plate. Ocean Eng 121:24–36. https://doi.org/10.1016/j.oceaneng.2016.05.009

54. Suja-Thauvin L, Krokstad JR, Bachynski EE, de Ridder EJ (2017) Experimental results of a multimode monopile offshore wind turbine support structure subjected to steep and breaking irregular waves. Ocean Eng 146:339–351. https://doi.org/10.1016/j.oceaneng.2017.09.024

55. Suja-Thauvin L, Krokstad JR, Bachynski EE (2018) Critical assessment of non-linear hydrodynamic load models for a fully flexible monopile offshore wind turbine. Ocean Eng 164:87–104. https://doi.org/10.1016/j.oceaneng.2018.06.027

56. Sun C (2018) Semi-active control of monopile offshore wind turbines under multi-hazards. Mech Syst Signal Process 99:285–305. https://doi.org/10.1016/j.ymssp.2017.06.016

57. Tödter S, el Sheshtawy H, Neugebauer J, Ould M, Thomas ES (2021) Deformation measurement of a monopile subject to vortex-induced vibration using digital image correlation. Ocean Eng 221:108548. https://doi.org/10.1016/j.oceaneng.2020.108548

58. van der Tempel, J (2006) Design of support structures for offshore wind turbines. 1st edn. Delft, The Netherlands

59. Wei K, Myers AT, Arwade SR (2017) Dynamic effects in the response of offshore wind turbines supported by jackets under wave loading. Eng Struct 142:36–45. https://doi.org/10.1016/j.engstruct.2017.03.074

60. Xie F, Aly A-M (2020) Structural control and vibration issues in wind turbines: a review. Eng Struct. https://doi.org/10.1016/j.engstruct.2019.110087

61. Yang Y, Bashir M, Li C, Michailides C, Wang J (2020) Mitigation of coupled wind-wave-earthquake responses of a 10 MW fixed-bottom offshore wind turbine. Renew Energy 157:1171–1184. https://doi.org/10.1016/j.renene.2020.05.077

62. Zdravkovich MM (1996) Different modes of vortex shedding: an overview. J Fluids Struct 10:427–437. https://doi.org/10.1006/jfls.1996.0029

63. Zhao M, Pearcey T, Cheng L, Xiang Y (2017) Three-dimensional numerical simulations of vortex-induced vibrations of a circular cylinder in oscillatory flow. J Waterw Port Coast Ocean Eng 143:04017007. https://doi.org/10.1061/(ASCE)WW.1943-5460.0000391

64. Zuo H, Bi K, Hao H (2017) Using multiple tuned mass dampers to control offshore wind turbine vibrations under multiple hazards. Eng Struct 141:303–315. https://doi.org/10.1016/j.engstruct.2017.03.006